JOURNAL OF RESEARCH of the National Bureau of Standards—C. Engineering and Instrumentation
Vol. 69C, No. 4, October–December 1965

Stress Analysis of Tape-Wound Magnet Coils*

Jesse Hord

Institute for Materials Research, National Bureau of Standards, Boulder, Colo.

(June 14, 1965)

A liquid hydrogen cooled, tape-wound, axially segmented, high-purity aluminum electromagnet has been built and tested to 95 kilogauss with a magnet power consumption of 22 kilowatts. Formulae for the axial, radial, and circumferential stress components in this type coil are derived under the assumptions of isotropy and homogeneity. Both plane strain and plane stress analyses are given. The hoop stress is also derived from the "floating shell" concept using thin shell theory. The formulae from these analyses and thick-wall cylinder theory are used to calculate the hoop stresses in the experimental coil, and the results are presented for comparison. The theoretical burst field of a monolithic cylindrical coil disk is derived.

Key Words: Axial stress, burst field, circumferential stress, cryogenic electromagnets, electromagnets, magnetic body forces, magnetic field, plane strain, plane stress.

1. Introduction

Many current research programs require the application of high magnetic fields. Plasma containment, heating, and acceleration are examples. Cryogenic electromagnets are rapidly becoming the most convenient, economical means of producing these high fields. Purcell and Payne [1][1] have discussed the advantages of cryogenic electromagnets and described in detail the coil construction treated herein.

The maximum field attainable with an electromagnet is limited by the mechanical strength of the coil. The field strength obtained with a given coolant system and magnet power supply may also be limited by the heat transfer efficiency and heat capacity of the coolant and the conductor resistivity. Therefore, optimum coil design requires simultaneous consideration of stresses, heat transfer, and conductor resistivity. The first of these is of sufficient importance to be treated separately in this paper.

In high-field magnets, the mechanical stresses may burst the coil. The coil may also fail by localized yielding which can result in increased coil resistance and electrical shorting. Therefore, it is necessary to determine the stress field for a specific magnet construction. The coil construction of particular interest here is the stack of tape-wound epoxy-bound cylindrical disks. The coil disks are alternately stacked with fiber disks which provide electrical insulation and sector-like openings for radial coolant passages. The stack of coil disks and separators is shown on figure 1. This photograph was taken following electrical and intermediate structural failure of the magnet

*This study was conducted on Contract AT–(49–2)–1165 for the U.S. Atomic Energy Commission, PROJECT SHERWOOD.
[1] Figures in brackets indicate the literature references at the end of this paper.

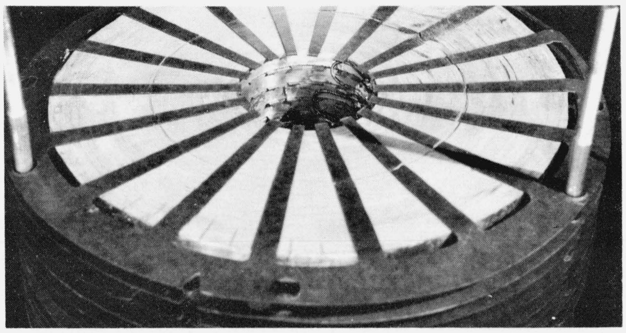

FIGURE 1. *Stack of magnet coil disks and disk separators with top four coil disks removed (after electrical and intermediate structural failure of the magnet at 95 kG).*

at 95 kilogauss (kG). The foil conductor is assumed to be tightly wound with alternate layers of paper insulation and then vacuum impregnated with epoxy resin to form a monolithic cylindrical disk. The paper and epoxy combined are not permitted to exceed 5 percent of the disk volume. The epoxy-paper tensile and compressive yield strengths exceed those of the conductor. This construction technique yields to the simplified analysis of an isotropic, homogeneous cylindrical disk. Although the epoxy-bound laminated construction cannot be perfectly isotropic, the assumption of isotropy is considered representative of the coil construction. These cylindrical coil disks are analyzed herein and formulae are developed for the axial, radial, and circumferential stress components. The radial and circumferential stress components are derived under the assumptions of both plane stress and plane strain. The hoop stress is also developed from the "floating shell" concept which assumes that each turn of the coil disk is an individual thin wall cylinder. This type analysis should be appropriate for loosely wound, poorly bonded coil disks. The formulation for predicting the burst field of a monolithic cylindrical coil disk is also developed. Stress and burst field design curves based on the analyses are presented.

Magnet stresses have been given considerable attention in the literature. For the most part, only the circumferential (hoop) stress component has been examined. This is reasonably justifiable since the circumferential stress is the largest component. Post and Taylor [2] point out that the magnetic pressure is proportional to $B_z^2/8\pi$, where B_z is the axial field component. They show that the main incremental body forces are proportional to the radial derivative of the magnetic pressure. Bitter [3] extends the magnetic pressure concept to a very useful form by assuming the coil to be a thick wall cylinder with internal pressure $B_0^2/8\pi$ (B_0 is the field at the geometric center of the coil). This calculation scheme is quick and easy to use and, as will be shown later, provides a rough estimate of the coil hoop stresses. However, it should be noted that this calculation scheme is valid only for the hoop stress (σ_c) component. If a shear failure theory is to be assumed for the coil, it is necessary to also know the axial (σ_z) and radial (σ_r) stress components. If the maximum normal stress failure theory is employed, then σ_c will suffice. It will be shown herein that σ_z is not negligible and can cause coil failure or excessive deformation under the disk separators.

Detailed stress analyses for various type magnets have been given by Cockcroft [4], Daniels [5], Giauque and Lyon [6], and Wells et al., [7]. None of these are deemed applicable to the magnet construction of interest for the following reasons: Cockcroft [4] assumed that the magnetic body forces were balanced at the outer periphery by an external pressure. This may be true for coils rigidly reinforced at the outer edge but no reinforcement was used for the coils described here. Cockcroft also made the simplifying assumption that the solenoid was a homogeneous, isotropic body, but neglected the largest stress component (σ_c) in his analysis. In addition, the formulae developed are dependent upon the calculation of the mutual inductance of a solid coil and a circle in the end plane. Although tables are given for specified variations in coil geometrical parameters, the calculation is laborious. Daniels [5] also utilizes the mutual inductance of one turn with the entire coil to derive stress formulae for coils fabricated by stacking tape-wound cylindrical disks. Since the disks were not considered to be structurally reinforced, the problem is similar to the one under consideration in this paper. Daniels [5] considered the problem as two dimensional and ignored stresses in the axial (Z) direction. The windings are assumed to be homogeneous and anisotropic because the coil was fabricated with nylon insulation between adjacent turns, and the composite was not integrally bonded in any way. It is assumed that the coil cannot unwind due to friction between adjacent turns. Daniels [5] includes the all-important hoop stress and the conditions of stress compatibility in the analysis. It is concluded that each turn of the coil is in equilibrium under its own body forces and that axial compression does not affect the magnitude of the stresses in the radial and circumferential directions. Daniels [5] also concludes that evaluation of the formulae developed is very laborious and suggests experimentation with models as an alternative to calculating the stresses. Giauque and Lyon [6] treat the problem of helical-wound cylindrical coils. Each helical layer of the solenoid was separated by an electrical insulating material which also defined the cooling fluid annuli. Thus, the coil could not provide uniformly distributed resistance to radial forces and was prevented from unwinding only by frictional drag or deformation of the conductor. Each helical layer of the coil is assumed to be self-supporting until the stresses in the conductor exceed the conductor yield strength. Giauque and Lyon [6] also use the mutual inductance method in the development of formulae for the axial and circumferential stress components. A simplified expression for the calculation of the mutual inductance between current element and coil is given for nonhomogeneous coils. This simplified expression is reported to be useful for the quick evaluation of maximum stresses in a design feasibility study. Under the foregoing assumptions Giauque and Lyon [6] neglect the radial stress component, assume a maximum normal strain failure theory, utilize the mathematical expression for calculating mutual inductance, and derive very useful equations for the hoop, axial, and failure stresses in unbonded helical-layer cylindrical coils. Wells et al., [7] have extensively examined the distribution of magnetic forces in toroidal solenoids. Wells [8] has also developed very useful formulae for the computation of hoop and radial stresses in Bitter magnets (current density is inversely proportional to the coil radius). The stress formulae developed herein are dependent upon the magnetic flux density (B). The recent data of Brown et al., [9, 10] provide numerical values of B for any solenoid. Therefore, stress calculations using the derived expressions are simplified.

2. Analysis

2.1 Nomenclature

B = vector magnetic flux density
B_0 = magnetic flux density at the geometric center of the coil
C = constant of integration
E = Young's modulus of elasticity
F = force generated by magnetic field
I = current per turn of conductor
J = current density in conductor
L = half length of cylindrical coil
m = absolute value of the slope of B_z/B_0 versus γ plot
N = number of turns in coil
p_m = magnetic pressure
r = radius at some turn in the coil (radial coordinate)
r_i = inside radius of coil
r_0 = outside radius of coil
t = wall thickness of a thin cylinder
u = measure of radial displacement
V = conductor volume
y = absolute value of B_z/B_0 at $r=r_i(\gamma=1)$
Z = denotes distance along axis from center of coil (axial coordinate).

a. Greek

α = ratio of outer to inner coil radius ($=r_0/r_i$)
β = ratio of coil half length to inner coil radius ($=L/r_i$)
γ = ratio of turn radius to coil inner radius ($=r/r_i$)
ϵ = unit strain in conductor
θ = circumferential coordinate
μ = Poisson's ratio
σ = unit stress in conductor

σ_y = yield stress of conductor

Φ = magnetic flux geometry parameter

$$\left\{ \equiv \frac{\beta}{\alpha - 1} \ln \left(\frac{\alpha + \sqrt{\alpha^2 + \beta^2}}{1 + \sqrt{1 + \beta^2}} \right) \right\}.$$

b. Subscripts

c = denotes circumferential direction

r = denotes radial direction

z = denotes axial direction

c. Superscripts

$*$ = denotes plane strain condition

Λ = denotes maximum (peak) value

— = denotes average value.

The analysis is performed under the following general assumptions: (1) The tape-wound, epoxy-bound axially segmented cylindrical coil is considered to be homogeneous and isotropic in each disk. (2) The radial and circumferential stresses are derived under the assumptions of plane stress and plane strain. The coil is comprised of a stack of relatively thin disks which are separated by a disk-shaped insulating material with sector-like openings for coolant flow. Therefore, it would be extremely difficult to exactly determine the effect of axial compression on the radial and hoop stresses. The assumption of plane stress is judged most applicable since the major portion of each disk face is exposed to coolant. Axial stresses due to axial magnetic force are transmitted from disk-to-disk via the spokes in the disk separators. The axial compression is magnified by the reduction in compression area under the disk separators. (3) The coil is symmetrical with symmetrical flux distribution and uniform current density. (4) Frictional drag under the spokes of the disk separators does not resist radial deformation of the conductor. (5) Buckling or warping of the disk does not occur. This also means that no bending takes place between spokes of the disk separators (due to axial compression). (6) The stress formulae developed are applicable only so long as the conductor stress remains below the proportional limit. (7) The maximum normal stress failure theory is chosen because the hoop stress component dominates. The maximum normal strain or maximum shearing stress failure theory is more applicable to the conductor material immediately below the separator spokes; however, the material under the spokes comprises a small portion of the disk volume, and the high compressive stresses can be redistributed to the unstressed conductor.

Consider the cross section of a coil with a magnetic flux linkage as shown in figure 2a. The horizontal (radial) component (1) of the vector field induces vertical (axial) forces on the conductor. The axial component (2) of the magnetic field induces radial forces on the conductor. The distribution of the axial field component across the solenoid radius is shown on figure 2b. The field variation along the solenoid axis is shown in figure 2c and the radial field distribution on figure 2d. The axial field creates the bursting effect and varies almost linearly across the coil radius. The radial field is nearly sinusoidal over the coil radius and increases with distance along the axis (Z) for $Z < L$. Now the incremental force on a conductor segment in a magnetic field is given as

$$\frac{dF}{dV} = \frac{BJ}{10}. \tag{1a}$$

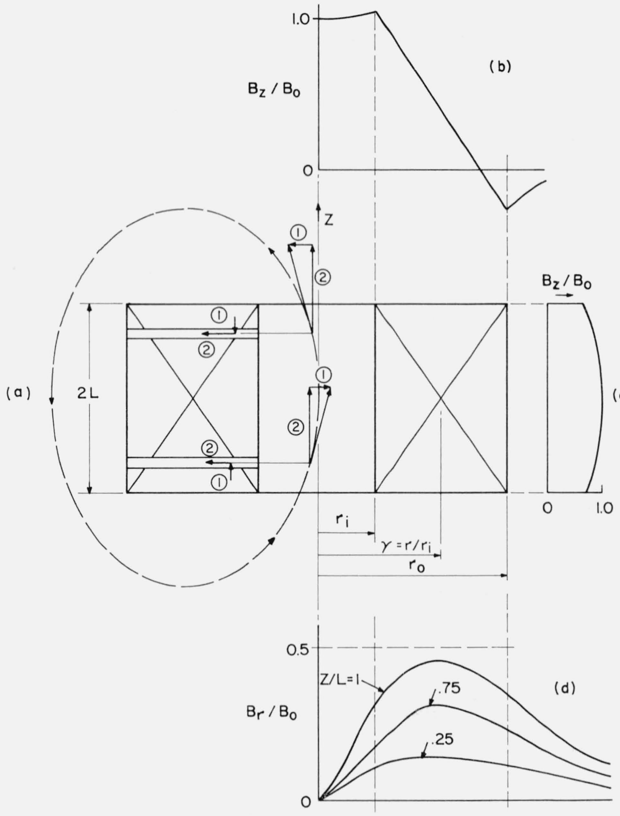

FIGURE 2. *(a) Cross section of solenoid showing magnetic flux components and associated body forces. (b) Distribution of the axial field component over the coil radius. (c) Distribution of the axial field component over the coil axis. (d) Variation of the radial field component with radial and axial position.*

The current density for the solenoid in figure 2a is

$$J=\frac{NI}{2L(r_0-r_i)}. \tag{1b}$$

Also, the field at the geometric center of the coil may be written,

$$B_0=\frac{4\pi NI}{10(2L)}\,\Phi. \tag{1c}$$

Combining eqs (1a), (1b), and (1c) we obtain the magnetic body force per unit volume of conductor;

$$\frac{dF}{dV}=\frac{BB_0}{4\pi(r_0-r_i)\Phi}. \tag{2a}$$

The radial force component is

$$\frac{dF_r}{dV}=\frac{B_zB_0}{4\pi(r_0-r_i)\Phi}, \tag{2b}$$

and the axial force component is

$$\frac{dF_z}{dV}=\frac{B_rB_0}{4\pi(r_0-r_i)\Phi}. \tag{2c}$$

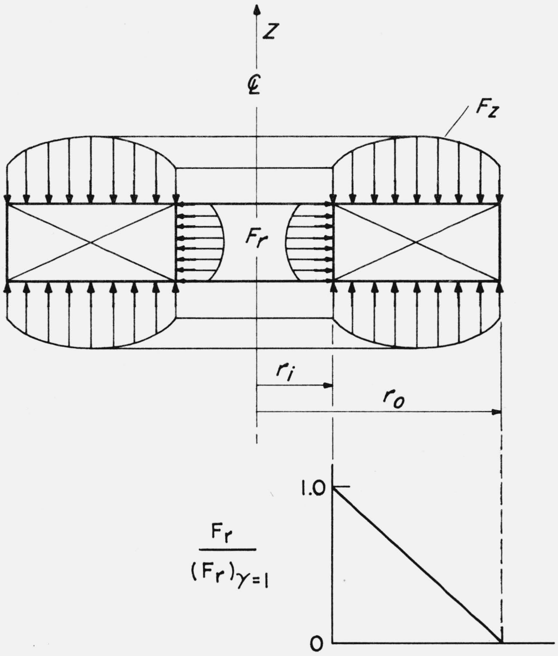

FIGURE 3. *Distribution of magnetic body forces on a coil disk at midplane* (Z/L=0).

Equations (2b) and (2c) are valid for any point in the coil cross section. Equations (2b) and (2c) indicate that the radial and axial forces are linearly proportional to the field components. Referring to the field distributions in figure 2, we can sketch the loading imposed on a typical disk in the coil. The distribution of the magnetic body forces is illustrated on figure 3.

Radial equilibrium of a differential element of conductor with magnetic body force $\frac{dF_r}{dV}$ is satisfied by

$$\sigma_c - \sigma_r - r\frac{d\sigma_r}{dr} = r\frac{dF_r}{dV}. \tag{3}$$

See Timoshenko and Goodier [11].

2.2. Plane Stress

For the condition of plane stress $\sigma_z = 0$. Hooke's law for the condition of plane stress may be written [12] in terms of stress and displacement as follows:

$$\sigma_c = \frac{E}{(1-\mu^2)}\left\{\frac{u}{r} + \mu\frac{du}{dr}\right\}, \tag{4a}$$

$$\sigma_r = \frac{E}{(1-\mu^2)}\left\{\frac{du}{dr} + \mu\frac{u}{r}\right\}. \tag{4b}$$

Combining eqs (3) and (4) we obtain the equilibrium equation in terms of displacement

$$\frac{d^2u}{dr^2} + \frac{1}{r}\frac{du}{dr} - \frac{u}{r^2} = -\left(\frac{dF_r}{dV}\right)\frac{(1-\mu^2)}{E}. \tag{5}$$

Equation (2b) must now be evaluated in order to solve this differential equation. It will be shown later that $B_z = B_0\left(\frac{r_0 - r}{r_0 - r_i}\right)$ provides fair results in computing the stresses at the midplane; however, to maintain generality we shall let

$$B_z = B_0[y + m(1-\gamma)], \tag{6a}$$

where y = the value of B_z/B_0 at $r = r_i$ (fig. 2b), and m = absolute value of the slope of B_z/B_0 (fig. 2b). Combining eqs (2b) and (6a) we obtain

$$\frac{dF_r}{dV} = \frac{B_0^2[y + m(1-\gamma)]}{4\pi(r_0 - r_i)\Phi}. \tag{6b}$$

Substitution of eq (6b) into eq (5) yields

$$\frac{d^2u}{dr^2} + \frac{1}{r}\frac{du}{dr} - \frac{u}{r^2} = K[y + m(1-\gamma)], \tag{7a}$$

where

$$K \equiv -\frac{B_0^2(1-\mu^2)}{4\pi E r_i(\alpha - 1)\Phi}. \tag{7b}$$

The left side of eq (7a) is recognized as Euler's equation and the complementary solution is written

$$u_1 = C_1 r + \frac{C_2}{r}. \tag{8a}$$

The particular solution to eq (7a) is

$$u_2 = Kr^2\left\{\frac{(y+m)}{3} - \frac{mr}{8r_i}\right\}, \tag{8b}$$

and $u = u_1 + u_2$. The constants of integration C_1 and C_2 are evaluated from the boundary conditions $\sigma_r = 0$ at the inner and outer radii of the disk. Invoking these boundary conditions and combining eqs (4b) and (8) we obtain

$$C_1 = -\frac{KQ_1 r_i}{24},\ C_2 = -\frac{KQ_2 r_i^3}{24},$$

where $Q_1 \equiv \left(\frac{1}{1+\mu}\right)\{Q_2(1-\mu) + 8y(\mu+2) + m(7+5\mu)\}$, and

$$Q_2 \equiv \left(\frac{\alpha^2}{\alpha^2 - 1}\right)\left(\frac{1}{\mu - 1}\right)\{8y(\mu+2)(1-\alpha) + m[(7+5\mu) - 8\alpha(\mu+2) + \alpha^2(9+3\mu)]\}.$$

Substituting into eqs (4) we obtain the following formulae;

$$\sigma_c = \frac{B_0^2}{96\pi(\alpha-1)\Phi}\left\{Q_1(1+\mu) + Q_2\frac{(1-\mu)}{\gamma^2} + 3m\gamma^2(1+3\mu) - 8\gamma(y+m)(1+2\mu)\right\}, \tag{9a}$$

$$\sigma_r = \frac{B_0^2}{96\pi(\alpha-1)\Phi}\left\{Q_1(1+\mu) - Q_2\frac{(1-\mu)}{\gamma^2} + 3m\gamma^2(\mu+3) - 8\gamma(y+m)(\mu+2)\right\}. \tag{9b}$$

The stresses are in dynes/cm² when B_0 is expressed in gauss. To convert to psi multiply $B_0^2 \times 14.5 \times 10^{-6}$.

784-657 O-65-4

2.3. Plane Strain

For the case of plane strain $\epsilon_z = 0$. Pursuing the method used in deriving the plane stress formulae we obtain for plane strain,

$$\sigma_c^* = \frac{B_0^2}{96\pi(\alpha-1)(\mu-1)\Phi}\left\{Q_1^* - Q_2^* \frac{(1-2\mu)}{\gamma^2} + 8\gamma(y+m)(1+\mu) - 3m\gamma^2(1+2\mu)\right\}, \tag{10a}$$

$$\sigma_r^* = \frac{B_0^2}{96\pi(\alpha-1)(\mu-1)\Phi}\left\{Q_1^* - Q_2^* \frac{(2\mu-1)}{\gamma^2} + 8\gamma(y+m)(2-\mu) - 3m\gamma^2(3-2\mu)\right\}, \tag{10b}$$

where

$$Q_1^* \equiv -8y(2-\mu)\left(\frac{\alpha^2}{\alpha+1}+1\right) + m(7-2\mu)\left(\frac{1}{\alpha^2-1}\right) - \frac{m\alpha^2}{\alpha^2-1}\{8\alpha(2-\mu)$$

$$+3\alpha^2(2\mu-3)\}, \text{ and } Q_2^* \equiv \frac{\alpha^2}{(\alpha^2-1)(2\mu-1)}\{8y(2-\mu)(1-\alpha) + m[(7-2\mu) - 8\alpha(2-\mu)$$

$$-3\alpha^2(2\mu-3)]\}.$$

2.4. Simplified Plane Stress

If the hoop stress at the midplane only is desired for design calculations some simplifying assumptions can be made.

$$\text{Set } B_z = B_0\left(\frac{r_0 - r}{r_0 - r_i}\right),$$

which requires that $y = 1$ and $m = \dfrac{1}{\alpha-1}$ in eqs (9). The resultant equations are

$$\sigma_c = \frac{B_0^2}{96\pi(\alpha-1)\Phi}\left\{\psi_1(1+\mu) + \psi_2\left(\frac{1-\mu}{\gamma^2}\right) + \frac{3\gamma^2(1+3\mu)}{\alpha-1} - 8\gamma\left(\frac{\alpha}{\alpha-1}\right)(1+2\mu)\right\}, \tag{11a}$$

$$\sigma_r = \frac{B_0^2}{96\pi(\alpha-1)\Phi}\left\{\psi_1(1+\mu) - \psi_2\left(\frac{1-\mu}{\gamma^2}\right) + \frac{3\gamma^2(\mu+3)}{\alpha-1} - 8\gamma\left(\frac{\alpha}{\alpha-1}\right)(\mu+2)\right\}, \tag{11b}$$

where $\psi_1 \equiv \left(\dfrac{1}{1+\mu}\right)\left\{\psi_2(1-\mu) + 8(\mu+2) + \left(\dfrac{1}{\alpha-1}\right)(7+5\mu)\right\}$,

and $\psi_2 \equiv \left(\dfrac{1}{\mu-1}\right)\left(\dfrac{1}{\alpha-1}\right)\left(\dfrac{\alpha^2}{\alpha^2-1}\right)\{8\alpha(\mu+2) - \alpha^2(5\mu+7) - 3\mu - 9\}$.

2.5. Bitter Method

Bitter [3] has suggested the use of formulae for the thick-wall cylinder subjected to internal pressure $B_0^2/8\pi$. Utilizing this method we obtain for stresses at the coil midplane,

$$\sigma_c = \frac{B_0^2}{8\pi}\frac{1+(\alpha/\gamma)^2}{\alpha^2-1}, \tag{12a}$$

$$\sigma_r = \frac{B_0^2}{8\pi}\frac{1-(\alpha/\gamma)^2}{\alpha^2-1}. \tag{12b}$$

As mentioned earlier, eq (12b) is not applicable because the boundary condition at the inner radius is not satisfied.

2.6. Floating Shell Method

The magnet fabricated at NBS admitted annular cracks of light upon completion, indicating imperfect epoxy impregnation. Thus, it seems worthwhile to calculate the hoop stresses as if each conductor turn is self-supporting and unrestrained, but closed as in a thin wall cylinder. The magnetic pressure may be written

$$dp_m = \frac{dF_r}{dA} = \left(\frac{dF_r}{dV}\right) dr. \tag{13a}$$

Restricting this calculation to the midplane we set

$$B_z = B_0 \left(\frac{r_0 - r}{r_0 - r_i}\right),$$

$dr = t$, $dp_m = \Delta p_m$, and combine eqs (2b) and (13a) with thin shell theory to obtain

$$\sigma_c = \frac{B_0^2 \gamma(\alpha - \gamma)}{4\pi(\alpha - 1)^2 \Phi}. \tag{13b}$$

This hoop stress reaches a maximum at the radius $r = r_0/2$. Then by the floating shell method the maximum hoop stress

$$(\hat{\sigma}_c)_{\gamma=\frac{\alpha}{2}} = \frac{B_0^2}{16\pi\Phi}\left(\frac{\alpha}{\alpha - 1}\right)^2. \tag{14}$$

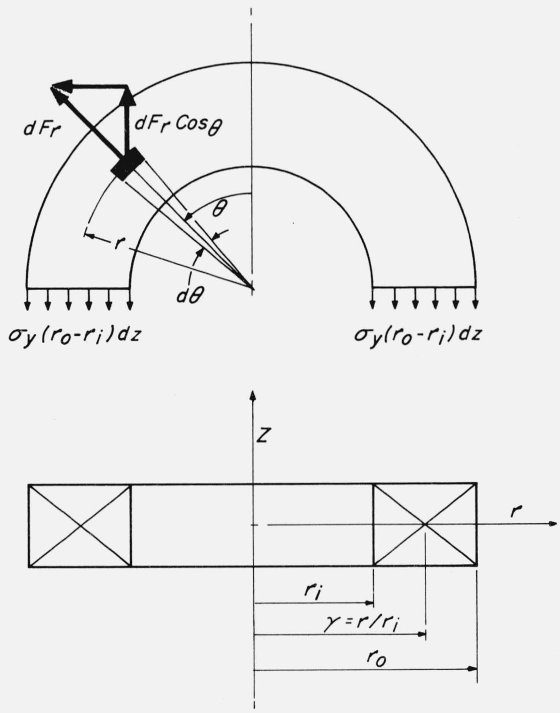

FIGURE 4. *Equilibrium of a coil disk when the entire cross section of the disk is stressed to the yield point.*

784-657 O-65-5

2.7. Burst Strength of Monolithic Disks

It is assumed that failure occurs when the coil material becomes plastic throughout. Although it has not yet been demonstrated, σ_z and σ_r are relatively low compared to σ_c, and therefore the maximum normal stress failure theory is selected. Referring to figure 4, equilibrium is satisfied when

$$2\sigma_y(r_0-r_i)dz=\int_V dF_r \cos\theta. \tag{15a}$$

Choosing unity thickness ($dz=1$) and combining eq (6b) and (15a) and performing the integration we obtain the theoretical bursting field

$$B_0^2=\frac{1.73(\alpha-1)^2\sigma_y\Phi}{(y+m)(\alpha^2-1)-\frac{2m}{3}(\alpha^3-1)}, \tag{15b}$$

where B_0 is in kG and σ_y in pounds per square inch.

If for the sake of simplicity we substitute $y=1$; $m=1/(\alpha-1)$ into eq (15b), the bursting field at the midplane is

$$B_0^2=\frac{5.2(\alpha-1)\sigma_y\Phi}{(\alpha+2)}. \tag{15c}$$

2.8. Axial Compression

The axial magnetic body forces are transmitted from disk to disk by the spokes of the disk separators. Thus, the forces are additive from the ends to the center so that the disk in the midplane must support the axial body forces of the entire coil. Axial equilibrium of a differential element requires that

$$\frac{d\sigma_z}{dz}=\frac{dF_z}{dV}. \tag{16}$$

In order to obtain σ_z we must evaluate $B_r(r, z)$ in eq (2c). It will be shown in the sample calculations which follow that the radial field component is approximated by an expression of the form

$$\frac{B_r}{B_0}=K_0+(\hat{K}-K_0)\left\{\sin\pi\left(\frac{\gamma-1}{\alpha-1}\right)\right\}, \tag{17a}$$

where $K_0\equiv\left\{\frac{(B_r/B_0)_{\gamma=1}+(B_r/B_0)_{\gamma=\alpha}}{2}\right\}$ for each Z/L of a fixed coil geometry, and $\hat{K}\equiv\left(\frac{B_r}{B_0}\right)_{\gamma=\frac{\alpha+1}{2}}$ (peak value of B_r/B_0 for each Z/L of a fixed coil geometry). K_0 and $\hat{K}-K_0$ can be linearly related to the axial dimension Z by;

$$K_0=m_1Z/L, \qquad \hat{K}-K_0=m_2Z/L, \tag{17b}$$

where m_1 is the slope of the K_0 versus Z/L plot, and m_2 is the slope of the $(\hat{K}-K_0)$ versus Z/L plot for a fixed coil geometry. Combining eqs (17a) and (17b) we obtain for the radial field,

$$\frac{B_r}{B_0}=\frac{Z}{L}\left\{m_1+m_2\sin\pi\left(\frac{\gamma-1}{\alpha-1}\right)\right\}. \tag{17c}$$

Combining eqs (2c), (16), (17c) and performing the integration the axial stress is derived,

$$\sigma_z = \frac{B_0^2 Z^2}{8\pi L r_i(\alpha-1)\Phi}\left\{m_1 + m_2 \sin \pi \left(\frac{\gamma-1}{\alpha-1}\right)\right\} + f(r) + C. \tag{18a}$$

Since external forces are not being considered $C=0$ and $f(r)$ is obtained from the boundary condition $(\sigma_z)_{Z=L}=0$. Performing the indicated algebra we arrive at a solution for the axial compressive stress

$$\sigma_z = -\frac{\beta B_0^2(L^2-Z^2)}{8\pi L^2(\alpha-1)\Phi}\left\{m_1 + m_2 \sin \pi \left(\frac{\gamma-1}{\alpha-1}\right)\right\}. \tag{18b}$$

This expression is applicable throughout the axial dimension of the coil. The axial stresses are largest at $Z=0$, and

$$(\sigma_z)_{Z=0} = -\frac{\beta B_0^2}{8\pi(\alpha-1)\Phi}\left\{m_1 + m_2 \sin \pi \left(\frac{\gamma-1}{\alpha-1}\right)\right\}. \tag{18c}$$

The radius at which $(\sigma_z)_{Z=0}$ becomes maximum is $\gamma = \frac{\alpha+1}{2}$. Assuming that each disk acts as a rigid plate so that the axial stress is equally distributed we find the average axial stress $(\bar{\sigma}_z)$ from

$$\bar{\sigma}_z = \frac{1}{\alpha-1}\int_1^\alpha \sigma_z d\gamma. \tag{19a}$$

Performing the indicated integration on eqs (18b) and (18c) we obtain

$$\bar{\sigma}_z = -\frac{\beta B_0^2(L^2-Z^2)}{8\pi L^2(\alpha-1)\Phi}\left\{m_1 + \frac{2m_2}{\pi}\right\}, \tag{19b}$$

and

$$(\bar{\sigma}_z)_{Z=0} = -\frac{\beta B_0^2}{8\pi(\alpha-1)\Phi}\left\{m_1 + \frac{2m_2}{\pi}\right\}. \tag{19c}$$

In order to obtain the maximum average compressive stress under the spokes of the disk separators at the midplane we need only to multiply the results of eq (19c) by the area magnification ratio $(A_{\text{disk}}/A_{\text{spokes}})$.

2.9. Sample Calculations

In order to compare the various formulae and illustrate their use, sample calculations are performed for the coil geometry of the NBS magnet.

$\alpha = \frac{r_0}{r_i} = 3.67$; $\beta = \frac{L}{r_i} = 1.87$; $r_i = 1.5$ in.; $r_0 = 5.5$ in.; $L = 2.8$ in.; $\mu = 0.33$ (aluminum); $\sigma_y = 4500$ psi; $\Phi = 0.64$. To evaluate eqs (9), (10), and (18c) we must determine the values of y, m, m_1, and m_2. All calculations will be performed for the midplane ($Z=0$) where the stresses are largest. All data for the radial and axial field components are taken from the tabulations of Brown et al., [9]. Brown and Flax [10] recently presented a graphical method for determining the magnetic field components of any finite coil by superposition of four semi-infinite solenoids. The axial field component (B_z/B_0) is plotted for various coil parameters (α, β) in figure 5. The dotted line indicates the extrapolated curve chosen to fit the coil parameters of the NBS magnet. Since β is shown to have little effect on the slope, the selection of the dotted line is based on linear extrapolation between the curves for $\alpha=3$ and $\alpha=4$. From figure 5 we obtain $y = 1.04$ and $|m| = 0.45$.

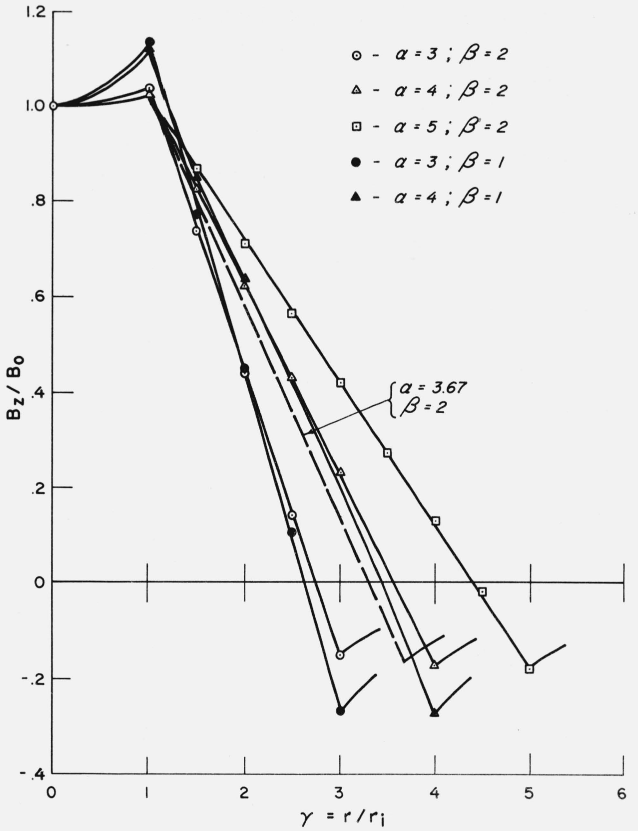

FIGURE 5. *Variation of midplane axial field with coil geometry.*

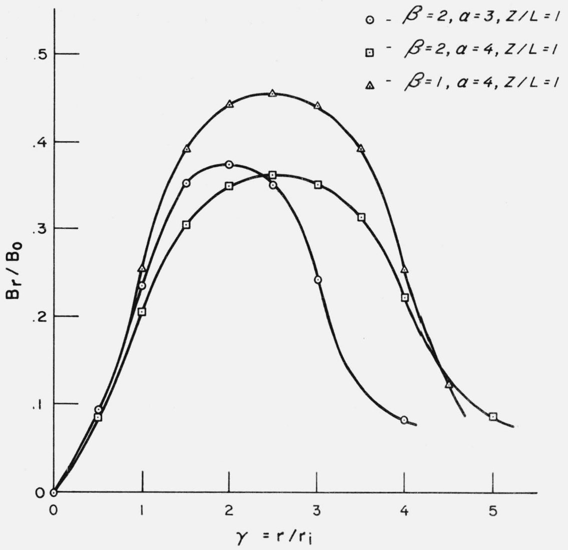

FIGURE 6. *Variation of end-plane radial field with coil geometry.*

On figure 6 is plotted the radial field component for various coil parameters. It is difficult to extend these curves to intermediate values of α and β. The effect of smaller β is to increase the magnitude of B_r/B_0 with little phase shift. Thus we plot on figure 7 the B_r/B_0 data for $\alpha=4, \beta=2$, and various Z/L. We note that the curves are essentially sinusoidal from $\gamma=1$ to $\gamma=4=\alpha$. Recalling that

$$K_0 \equiv \left\{\left(\frac{B_r}{B_0}\right)_{\gamma=1} + \left(\frac{B_r}{B_0}\right)_{\gamma=\alpha}\right\}\frac{1}{2},$$

and

$$\hat{K} \equiv \left(\frac{B_r}{B_0}\right)_{\gamma=\frac{\alpha+1}{2}},$$

we plot K_0 and $(\hat{K}-K_0)$ against Z/L on figure 8. From the K_0 plot we obtain the slope $m_1=0.213$, and from the $(\hat{K}-K_0)$ curve we obtain the slope $m_2=0.15$. Substituting these values of m_1 and m_2 into eq (17a) we check on the validity of the assumptions. The B_r/B_0 is calculated from eq (17a) and plotted on figure 7 for comparison. The calculated values plot high for lower values of Z/L; however, recall that the effect of a lower β (fig. 6) is to increase the B_r/B_0. Also, the fit is good for higher Z/L where the largest body forces are generated. The various formulae are evaluated and plotted for comparison on figure 9. From eqs (15b) and (15c) we calculate the bursting field as 93 kG and 84 kG, respectively. Using eq (19c) and an area magnification ratio of 4.4 we obtain

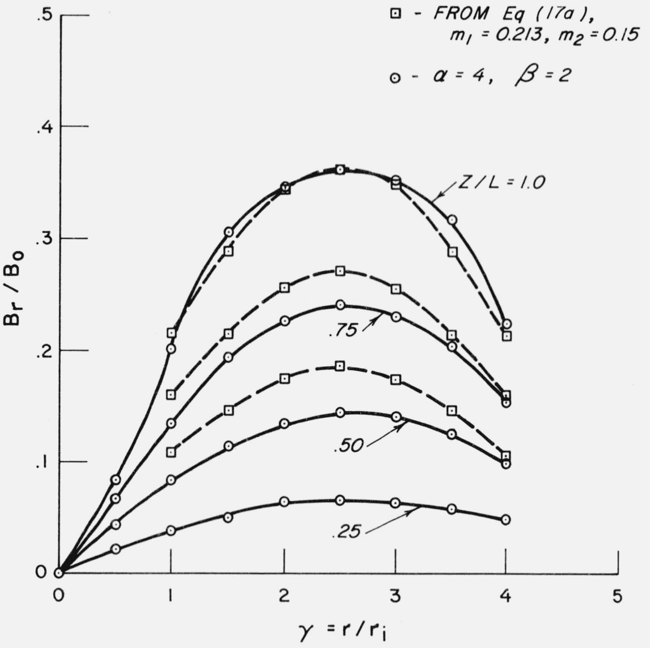

FIGURE 7. *Radial field as a function of axial position for a fixed coil geometry* ($\alpha=4$, $\beta=2$).

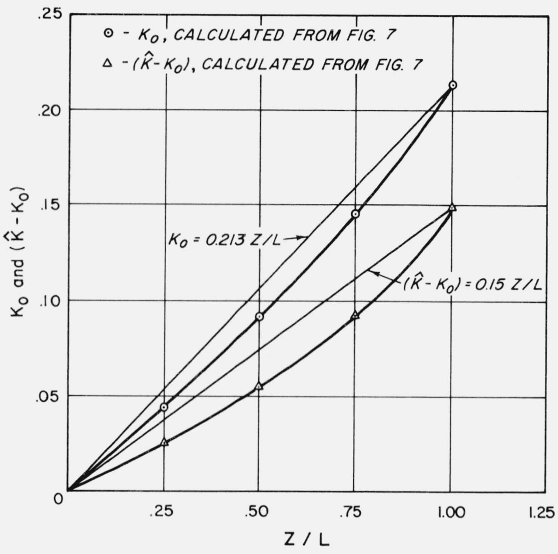

FIGURE 8. K_0 *and* $(\hat{K}-K_0)$ *as a function of axial position for a fixed coil geometry* ($\alpha=4$, $\beta=2$).

the average axial stress (psi) under the separator spokes as $-0.843\ B_0^2$ (B_0 in kG). The maximum hoop stress $[(\sigma_c)_{\gamma=1}$ from eq (11a)] is plotted for various coil parameters (α, β) on figure 10. Figure 11 shows the bursting field [B_0 from eq (15c)] as a function of α and β.

2.10. NBS Magnet Failure

The NBS tape-wound aluminum magnet failed electrically with intermediate structural damage at 95 kG. The magnet failure is attributed to excessive deformation at the outer radii which normally precedes bursting. Therefore, the failure field should not be much different from the actual burst field. The failure field agrees well with the 93 kG burst field calculated from eq (15b). The actual burst field is expected to exceed the theoretical value due to the frictional restraint of the axial compression (which was neglected in the analysis). Eight of the fourteen disks suffered circumferential cracks at radii of about 3.75 in. indicating excessive deformation at the outer radii and structural inhomogenieties. Some of the cracks were 0.125 in. wide. There is evidence of some radial deformation over the entire coil radii. The deformation of individual coil disks varied with coil axial position. The disks nearest the coil midplane were exposed to the largest magnetic pressure and suffered greater damage. The pronounced failure at an intermediate radius has been attributed to an intrinsic weakness in the coil disk construction. Several of the disks were rather loosely wound, and consequently some sizeable voids in the outer turns of the disk were epoxy-filled. All of the disks that failed possessed these voids from which the circumferential cracks propagated. Other disks in the coil had been tightly wound and suffered little or uniform stress damage. It would be quite difficult to determine what type structure the loosely wound epoxy-bound disk construction represents; however, it is estimated that the stresses should be intermediate to floating shell and plane stress analyses. The hoop stresses for the floating shell (eq (13b)) and simplified plane stress (eq (11a)) conditions are superimposed on the conductor yield strength

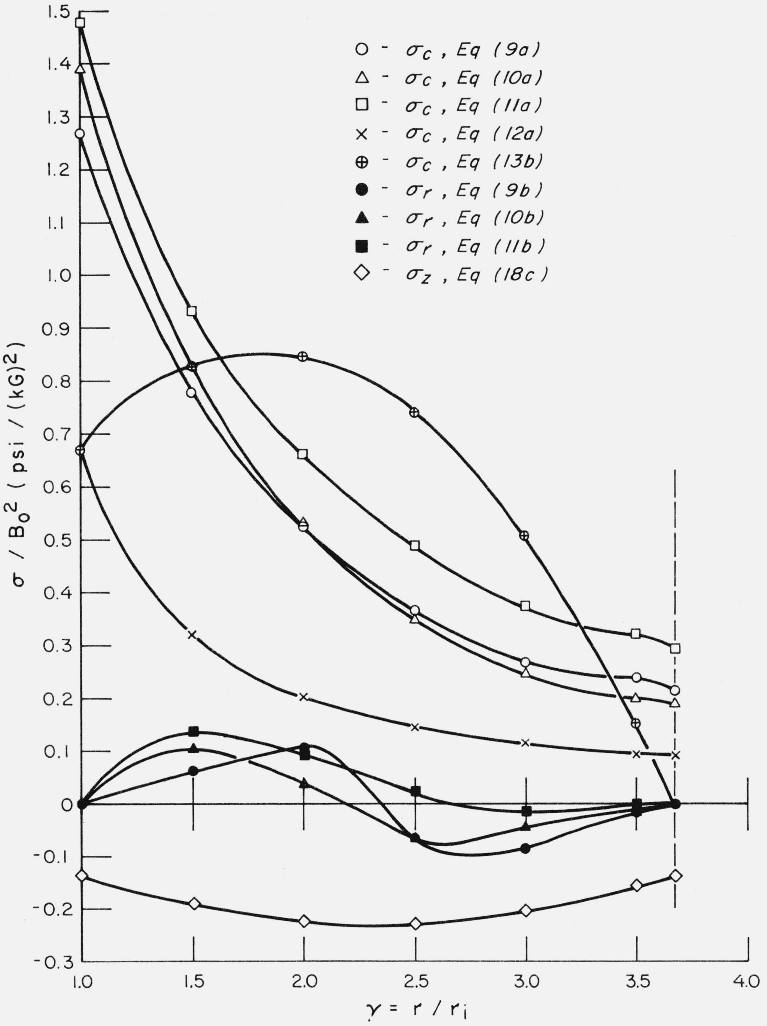

FIGURE 9. *Circumferential, radial and axial stress distributions at the midplane for the NBS magnet* ($\alpha=3.67$, $\beta=1.87$) *as computed from the various theories discussed.*

on figure 12. The variation in radii at which failure occurred is also indicated on figure 12. The conductor yield strength (0.2% offset) was experimentally determined to be 3300 psi at room temperature. The yield strength was then inferred to be 4500 psi at 20 °K (the operating temperature of the magnet). The actual strength of the material throughout the coil was unknown because the magnet had been tested at fields up to 70 kG several times prior to the 95 kG test. Thus, the material in the inner turns had been strain-hardened. Increased magnet resistance substantiated strain-hardening. The cyclic effect of strain on resistance and strength is under study; however, it is well known that the yield strength of pure aluminums can be increased three-fold at 20 °K by strain-hardening. A three-fold increase in yield strength of the inner turns of the coil disks would explain the circumferential cracks at intermediate radii when the magnetic field was increased from 70 to 95 kG. The epoxy voids provided the inherent weakness to permit the outer turns to expand radially outward from the strain-hardened inner turns. From figure 12 one could only conclude that the loosely wound turns of the epoxy-bound disks conformed more closely to the floating shell analogy. The shaded area on figure 12 indicates the region where the actual stresses for the loosely wound coils may plot. Some of the disks near the midplane were also badly damaged by axial compression. Extrusion of the conductor into the flow passages varied from 0.001

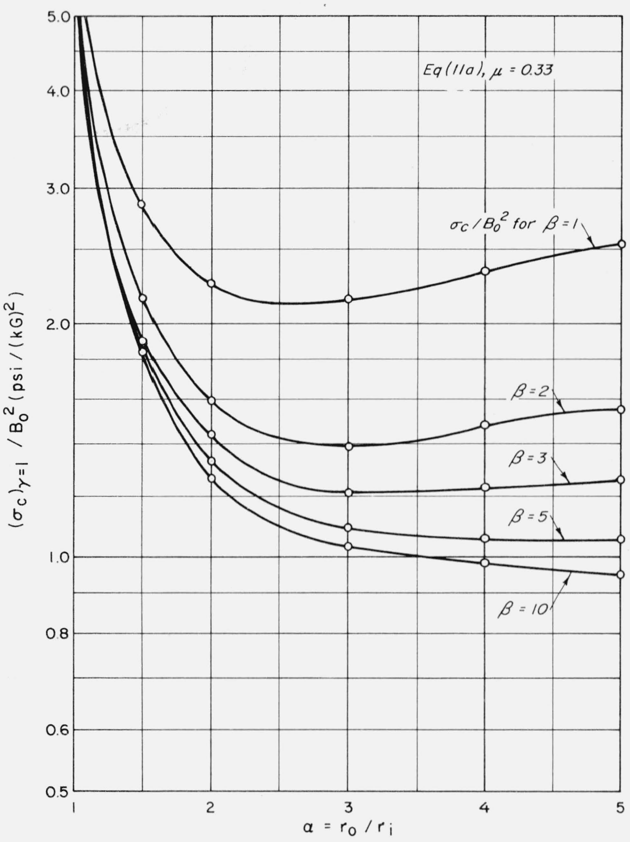

FIGURE 10. *Maximum hoop stress as a function of the coil parameters, α, β.*

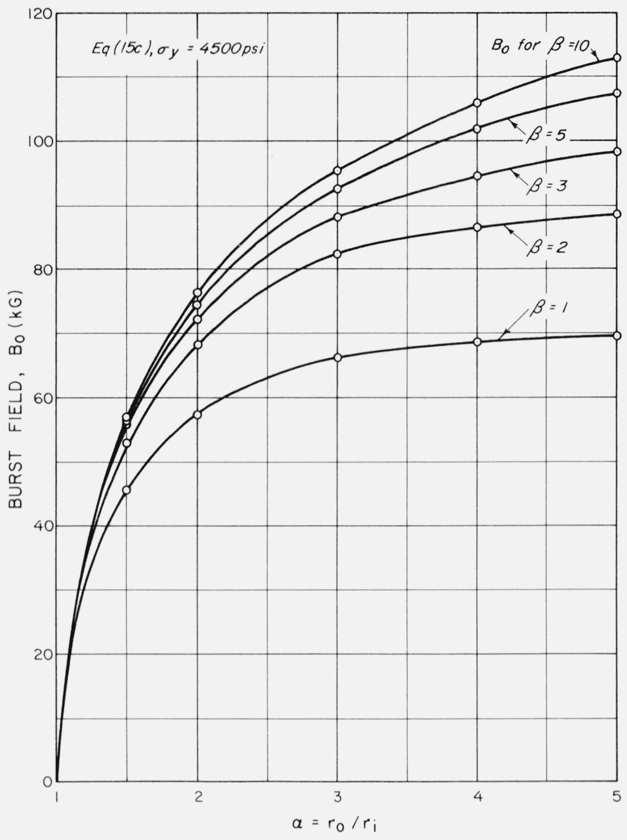

FIGURE 11. *Burst field as a function of the coil parameters, α, β.*

to 0.014 inches depending upon the disk axial position and the apparent aluminum-epoxy composite strength. Although the disks are separated by 0.025 inch fiber spacers a 0.004 in. feeler gage could not be inserted in some of the flow passages upon post-run inspection.

3. Conclusions

For quick design computations the method of Bitter, eq (12a), though nonconservative, is by far the most convenient. If a more precise analysis of both circumferential and axial stresses is desired eqs (9a) and (18c) are recommended. Equation (11a) is more convenient than eq (9a) and provides conservative results for hoop stress calculations.

Equation (13b) is suggested for hoop stress calculations on coils which are loosely wound and not integrally bound. The radial stress component is so small that it can be neglected in the coil construction described herein. Equation (11b) is recommended for those coil constructions where the radial stress is pertinent. Equation (15b) predicts the burst field of the tape-wound coil disks with reasonable precision. Equation (15b) and the simplified eq (15c) predict burst fields lower than those to be expected in practice. The actual burst field of a coil may be increased by strain-hardening the conductor through cyclic testing to the requisite fields.

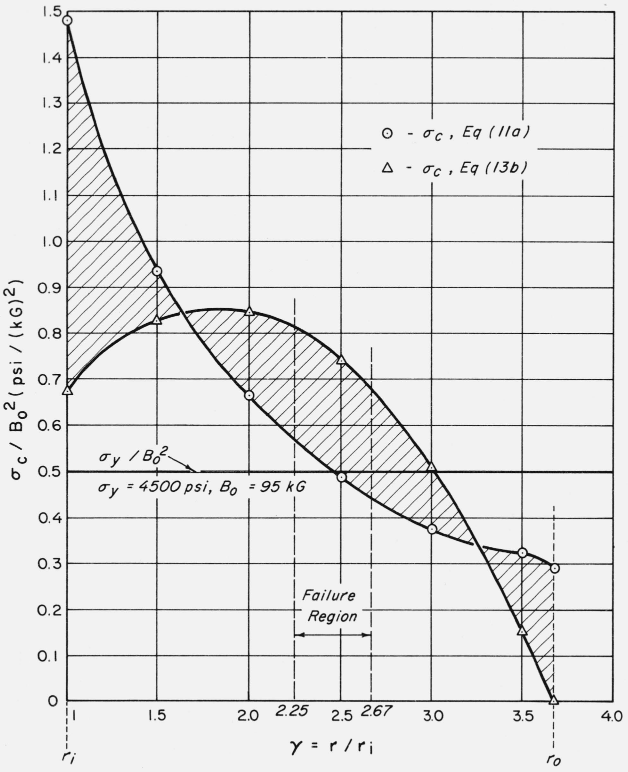

FIGURE 12. *Hoop stresses (as computed from the most dissimilar theories) and yield strength are superimposed on the failure radii of the NBS magnet.*

The author acknowledges the capable assistance of Larry L. Sparks and Jerry C. Jellison in performing the magnet experiments. Special recognition is due Vincent D. Arp for several fruitful discussions and ideas which are reflected throughout the text.

4. References

[1] J. R. Purcell and E. G. Payne, High-field liquid H_2-cooled aluminum-wound magnet, Rev. Sci. Instr. **34**, 893 (Aug. 1963).

[2] R. F. Post and C. E. Taylor, Air core cryogenic magnet coils for fusion research and high-energy nuclear physics Applications, Advan. Cryog. Eng. **5**, 13 (Plenum Press, Inc., New York, N.Y., 1960).

[3] F. Bitter, High Magnetic Fields, p. 85 (John Wiley and Sons, Inc., New York, N.Y., 1962).

[4] J. D. Cockcroft, The Design of coils for the production of strong magnetic fields, Phil. Trans. Roy. Soc. **227**, 317 (1928).

[5] J. M. Daniels, High power solenoids; stresses and stability, Brit. J. Appl. Phys. **4**, 50 (1953).

[6] W. F. Giauque and D. N. Lyon, Design of a 100-kilogauss 4-inch core solenoid for continuous operation, Rev. Sci. Instr. **31**, 374 (1960).

[7] D. R. Wells, R. G. Mills, A. Bahr, and R. L. Peskin, Project Matterhorn, Tech. Memo. No. III (1960), unpublished.

[8] D. R. Wells, Project Matterhorn, Tech. Memo. No. 30, NYO–6375 (1956), unpublished.

[9] Gerald V. Brown, Lawrence Flax, Eugene C. Itean, and James C. Laurence, Axial and Radial Magnetic Fields of Thick, Finite-Length Solenoids, NASA TR–R170 (December 1963).

[10] Gerald V. Brown and Lawrence Flax, Superposition of semi-infinite solenoids for calculating magnetic fields of thick solenoids, J. Appl. Phys. **35**, 1764 (June 1964).

[11] S. Timoshenko and J. N. Goodier, Theory of Elasticity, p. 58, 2d ed. (McGraw-Hill Book Company, Inc., New York, N.Y. 1951).

[12] S. Timoshenko, Strength of Materials, p. 207, 3d ed. (D. Van Nostrand Company, Inc., Princeton, New Jersey, 1956).

(Paper 69C4–210)